Testing theories of the vertical stratification of the ACC against observations

Richard H. Karsten [a,*], John Marshall [b]

[a] *Department of Mathematics and Statistics, Acadia University, Wolfville, NS, Canada B0P 1X0*
[b] *Department of Earth, Atmospheric and Planetary Sciences, Massachusetts Institute of Technology, Cambridge, MA 02139, USA*

Abstract

Recent theories of the Antarctic Circumpolar Current (ACC) suggest that its lateral and vertical stratification is controlled by its baroclinic instability: eddies in the ACC not only feed-off the available potential energy stored in sloping isopycnals but play a central role is setting up that stratification. Simple theory makes predictions about how the depth of the thermocline in the ACC depends on the surface winds, the air–sea buoyancy flux and transfer by baroclinic eddies. By examining gridded hydrographic data, here we test some of these predictions against observations. We show that, to a remarkable degree, the buoyancy field in the ACC decays exponentially with depth beneath the mixed layer. The e-folding depth increases equatorward, from less than 500 m on the poleward flank of the ACC to greater then 1000 m on its equatorial flank, in a manner that is broadly consistent with the theory.
© 2002 Elsevier Science B.V. All rights reserved.

1. Introduction

The Antarctic Circumpolar Current (ACC) is the only major current that circumnavigates the globe—see Fig. 1—and has many unique characteristics (see Rintoul et al., 2001 for a recent review). The ACC exists in thermal wind balance with isopycnals that slope up toward the pole, as shown in Fig. 2. The slope of the isopycnals is set, we believe, by a balance established between the surface winds which drive the 'Deacon Cell' overturning isopycnals and baroclinic eddies which extract potential energy and tend to flatten them out. This basic physical process and relevant theory is studied in an idealized modeling context in Karsten

---

* Corresponding author.
E-mail addresses: richard.karsten@acadiau.ca (R.H. Karsten), marshall@gulf.mit.edu (J. Marshall).
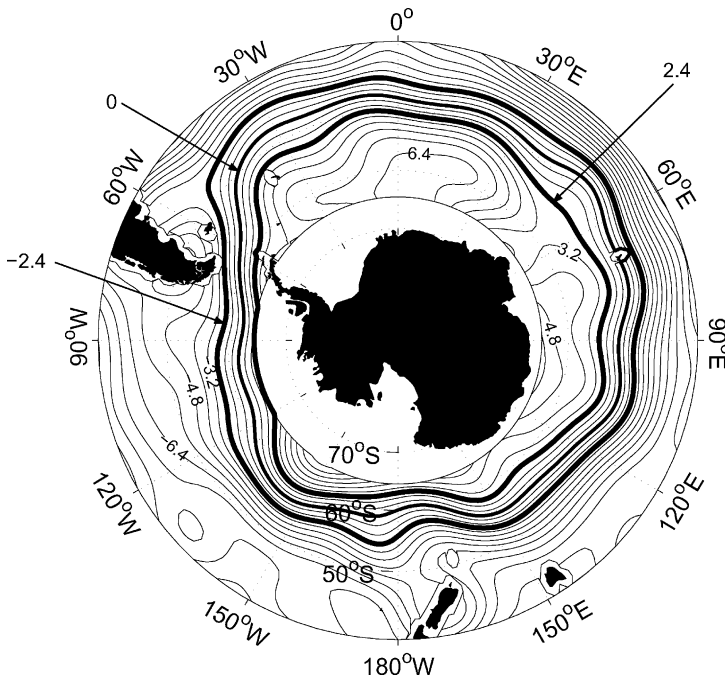
Fig. 1. The geostrophic streamlines, $\Psi_g = gh/f$, with g the gravitational acceleration, h the sea surface height from altimetry and f the Coriolis parameter. The contour interval is $0.8 \times 10^4\,\mathrm{m}^2\,\mathrm{s}^{-1}$ with the value increasing traveling poleward. The zero contour is located at the axis of the ACC. The bold solid lines mark the boundaries of circumpolar flow: $\Psi_g = \pm 2.4 \times 10^4\,\mathrm{m}^2\,\mathrm{s}^{-1}$.

et al. (2002) (hereafter KJM) and in a laboratory setting in Marshall et al. (2002). The theory makes predictions about the vertical stratification of the ACC and how it depends on wind, buoyancy forcing and transfer by baroclinic eddies. Here, we test those predictions against observations in the ACC. To characterize the vertical extent of the ACC, we make use of the observed equivalent barotropic (hereafter EB) structure of the ACC. The EB structure has been noted in both observations (Gordon et al., 1978; Marshall et al., 1993; Gille, 1995; Phillips and Rintoul, 2000) and analysis of numerical models (Killworth, 1992; Krupitsky et al., 1996; Ivchenko et al., 1996; Killworth and Hughes, 2002). This observation has led to a series of models which examine the path of the ACC using the EB simplification (see, for example, Killworth, 1992; Krupitsky et al., 1996; Ivchenko et al., 1996). Killworth and Hughes (2002) discuss in detail how the EB structure can be used to examine Welander's similarity solutions of the ideal fluid equations and describe the ACC path and structure. The approach allows the topography and its form-stress to enter the calculations in a natural manner. However, analytical progress depends on assuming separable EB form and does not explain how it arises or depends on external parameters.

Here, we examine the observed vertical stratification of the ACC using gridded hydrographic data. Firstly, we show that the stratification can be well-described by an exponential profile, but only if the e-folding scale (a measure of thermocline depth) is a function of
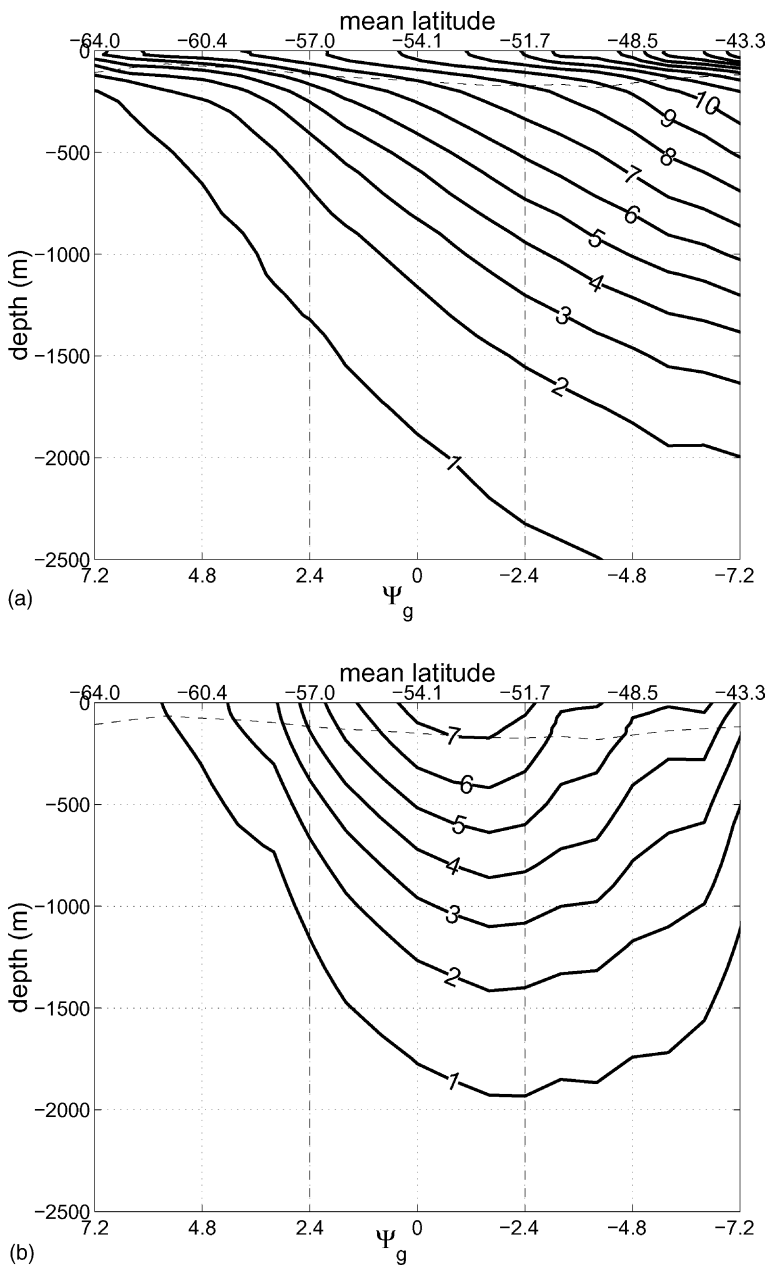
Fig. 2. (a) The mean streamwise-average buoyancy with contour interval $1 \times 10^{-3}\,\mathrm{m\,s^{-2}}$. (b) The mean streamwise-average thermal wind velocity with contour interval $1\,\mathrm{cm\,s^{-1}}$ obtained by assuming that the zonal flow at the bottom is zero and integrating up using thermal wind. The vertical dashed lines mark the boundaries of the ACC, the horizontal dashed line marks the annual mean mixed layer depth.

horizontal position: thus, a separable EB form seems to be a poor assumption for the mean buoyancy field of the ACC. Secondly, we study what processes might control the e-folding scale and examine how its variation depends on the balance of wind forcing and eddy fluxes.

In Section 2, we describe how we fit exponentials to the 'Levitus' climatology and map out the e-folding depth h_e. In Section 3, we put forward a simple theory that attempts to explain the observed distribution. In Section 4, we conclude.

2. Fitting an exponential to the vertical buoyancy profile

Using the gridded hydrographic data of Levitus and Boyer (1994) at $1°$ horizontal resolution, we calculate the buoyancy, b, at each latitude–longitude grid point using $b = -g\sigma/\rho_0$, where the potential density, σ, is calculated using a nonlinear equation of state (Gill, 1982) and $\rho_0 = 1030\,\mathrm{kg\,m^{-3}}$ is the average density of sea water. We then use a least square curve fitting routine to fit an exponential curve to the mean buoyancy below the annual mean mixed layer depth, h_m, given by Levitus and Boyer (1994). We assume the buoyancy has the form

$$\bar{b}(\theta, \phi, z) = \begin{cases} b_m(\theta, \phi), & -h_m(\theta, \phi) \le z \le 0 \\ \bar{b}_0(\theta, \phi)\exp[(z - h_m)/h_e], & -H \le z \le -h_m(\theta, \phi) \end{cases}, \qquad (1)$$
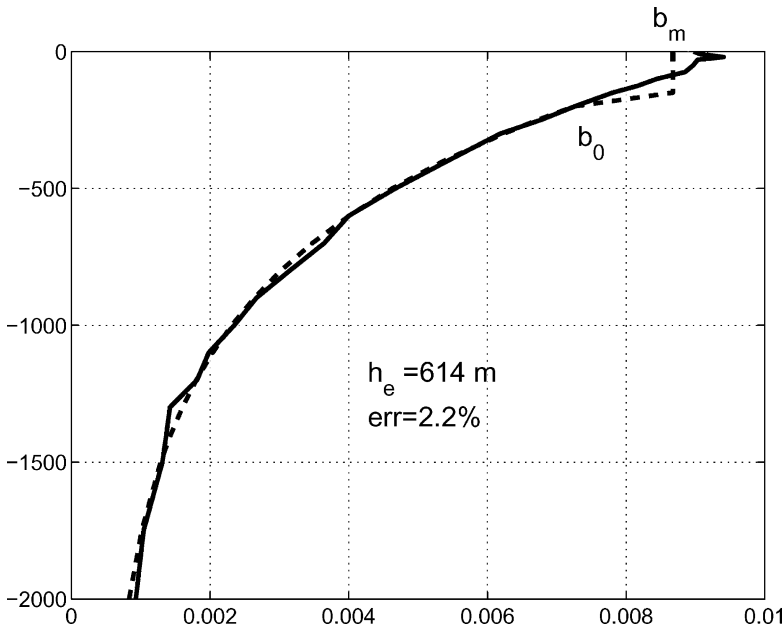

Fig. 3. The vertical structure of the buoyancy at 99.5°E, 50.5°S (solid line) with the approximation given by (1) (dashed line). The relative error in the fit at this location is 2.2%.

where h_e is the e-folding depth, $\bar{b}_m(\theta, \phi)$ the mixed layer buoyancy, (θ, ϕ) are the latitude and longitude, and z is the height, with $z = 0$ at the surface and $z = h_m(\theta, \phi)$ is the base of the mixed layer. The method minimized the error as measured by (2) and discussed below. In this manner we calculate the e-folding depth, h_e, of the buoyancy at each grid point. In Fig. 3, we show the $\bar{b}$ field at one particular point (99.5°E, 50.5°S) and the approximation given by (1): the best fit is obtained when $h_e = 614$ m.

In Fig. 4(a), we plot the calculated h_e at all horizontal columns in our domain. It is clear that h_e varies considerably in space. There are relatively high values to the north of the ACC and lower values to the south of the ACC. In the region of the ACC itself, h_e lies predominantly in the 500–1000 m range. In Fig. 4(b), we have also plotted the streamwise mean of h_e. The mean shows a striking increase across the ACC from a minimum of just
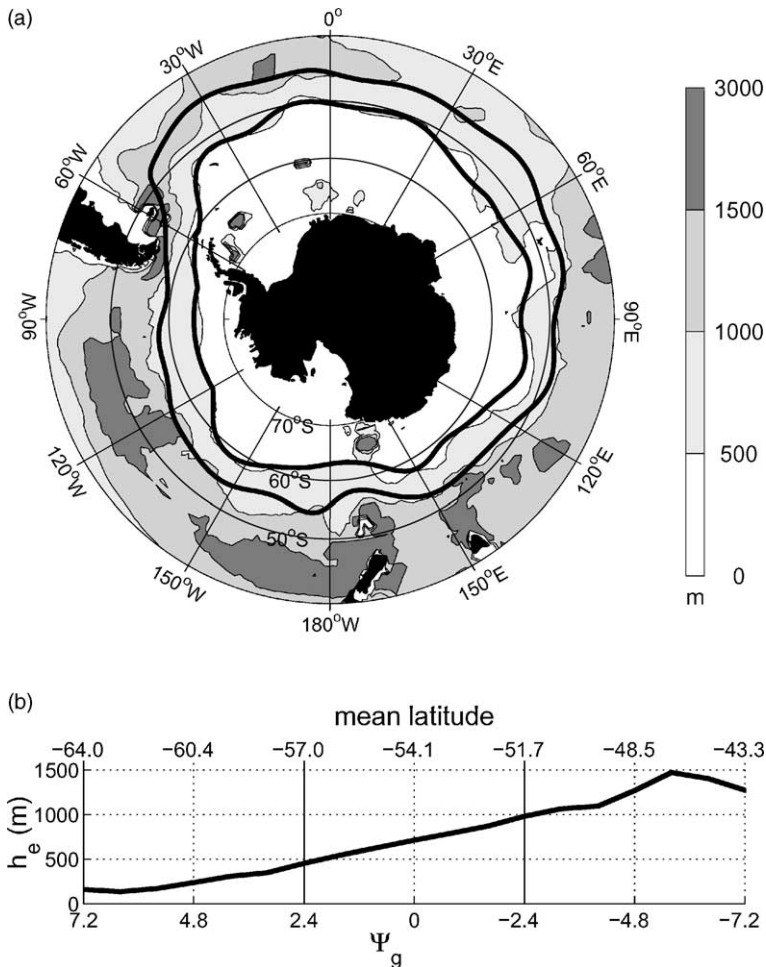

Fig. 4. (a) The e-folding depth, h_e, of the mean buoyancy in each column plotted as a function of position; (b) the along-stream average of h_e.

under 500 m at the polar boundary to in excess of 1000 m on the equatorial flank. As we will show in Section 3, this trend can be directly connected to the wind forcing. Note that over the typical 5° width of the ACC f varies by less than 10%, and even over the full range of the ACC, say 47–67°S, f varies by only 25%. Thus, the variations in the e-folding depth across the ACC are more marked than the variations in f.

One might question how accurately an exponential profile captures the vertical buoyancy structure. The numerical experiments of KJM suggest that the exponential profile should be accurate in regions of circumpolar flow, but perhaps not elsewhere in the Southern Ocean. We plot the relative error in the exponential fit in Fig. 5 given by

$$\text{error} = \frac{\sum[b(\theta, \phi, z) - b_{\text{m}}(\theta, \phi) \exp(z/h_{\text{e}})]^2}{\sum[b(\theta, \phi, z)]^2}, \tag{2}$$

where the sum is over depth. The thick lines indicate the bounds of circumpolar flow as determined by the mean streamlines obtained from altimeter data (see Fig. 1). The exponential profile indeed fits extremely well in the region of circumpolar flow, with an error of less than 5% and often less than 2.5%. In regions outside the ACC, however, the fit is not as good (errors often exceed 10%) and the exponential profile is at best a rough approximation of the vertical stratification. This emphasizes that the circumpolar nature of the ACC distinguishes it from the subtropical gyres of the Southern Ocean.
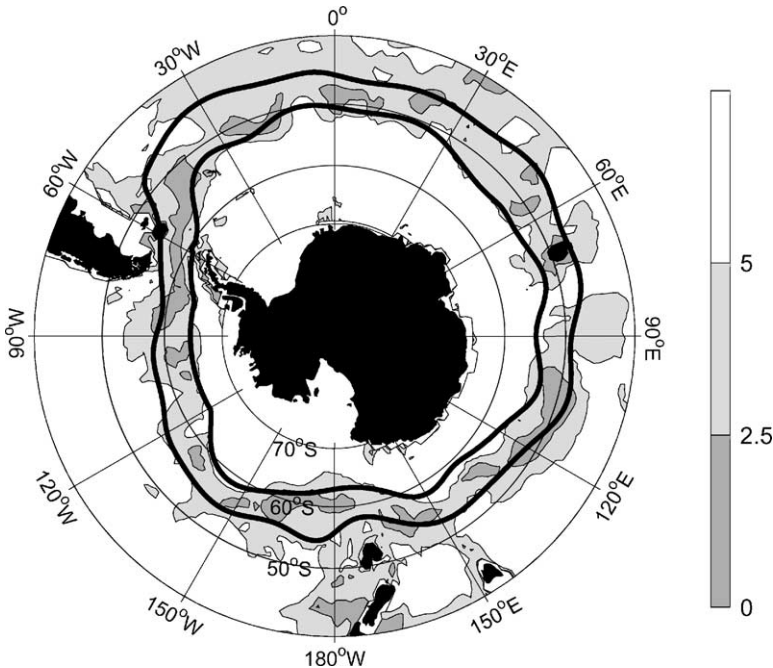

Fig. 5. The relative error (%) in the fit of the exponential profile, with e-folding depth shown in Fig. 4, as calculated using (2). North of the ACC, the error generally lies between 5 and 10%. South of the ACC, the error generally exceeds 10%.

The mean values of the e-folding depth in Fig. 4(b) are smaller than the 1600 m found in Marshall et al. (1993) for perhaps two main reasons (Gille, 1995 also predicts a deeper e-folding; depth of 1500 m). First, Marshall et al. (1993) included data to the north of the ACC where the thermocline is much deeper. Secondly, the logarithmic fit used in Marshall et al. (1993) emphasized bottom values by excluding all data above 400 m and preferentially weighted values at higher density. Here, by fitting an exponential curve we emphasize the region just below the mixed layer. Examining Marshall et al. (1993), it is clear that a fit to lower density values would decrease their e-folding to perhaps 800 m more in accord with the calculations presented here (Fig. 9(b)). Lastly, it should be noted that the FRAM model results predict a typical e-folding depth of 900 m (Krupitsky et al., 1996).

It should be noted that our results for the ACC are not dependent on the mixed layer depth. We have repeated the process with $h_m = 0, 50, 100, 200, 400$ m. Despite this large range, the streamwise-average e-folding depth over the range of the ACC varies by only ± 50 m. The error in the fit may increase by 1–2%, but the ACC is always clearly marked as the region of the lowest error. Outside the ACC, changing the mixed layer depth has a more dramatic effect, especially south of the ACC where the e-folding depth can change significantly if the highly stratified surface waters are included or excluded.

3. What sets the thermocline depth, h_e?

The focus of KJM was to understand the dependence of the stratification of the ACC on surface forcing and eddy transfer processes. In Karsten and Marshall (2002) (hereafter KM), we argued, using observations, that the leading order balance between winds and eddies found in KJM (and many other studies—see, e.g. Döös and Webb, 1994; Danabasoglu et al., 1994; Olbers and Ivchenko, 2001) does indeed hold at the northern boundary of the ACC. In KJM, we established simple connections between h_e and the surface forcing patterns which predicted plausible vertical scales for the ACC and were supported by the laboratory experiments of Marshall et al. (2002). Here, we show that these simple connections can also account for the cross-stream variation of h_e. In this section all averages are streamwise averages of time-mean quantities: h_e is the streamwise averaged e-folding depth given in Fig. 4(b) and y is the cross stream coordinate.

3.1. Residual buoyancy balance

The key equation in our analysis is the steady state, streamwise averaged buoyancy budget derived in Marshall (1997) and KJM. The budget holds in the mixed layer of depth h_m and is written in terms of a residual transport, Ψ_{res}, and the mixed layer buoyancy, $\bar{b}_m(y)$. In the steady state, the horizontal divergence of buoyancy transport—$\partial(\Psi_{res}\bar{b}_m)/\partial y$—minus the subduction of buoyancy at the mixed layer base—$(\partial\Psi_{res}/\partial y)\bar{b}_m$—must balance the surface buoyancy forcing of the mixed layer, B, yielding

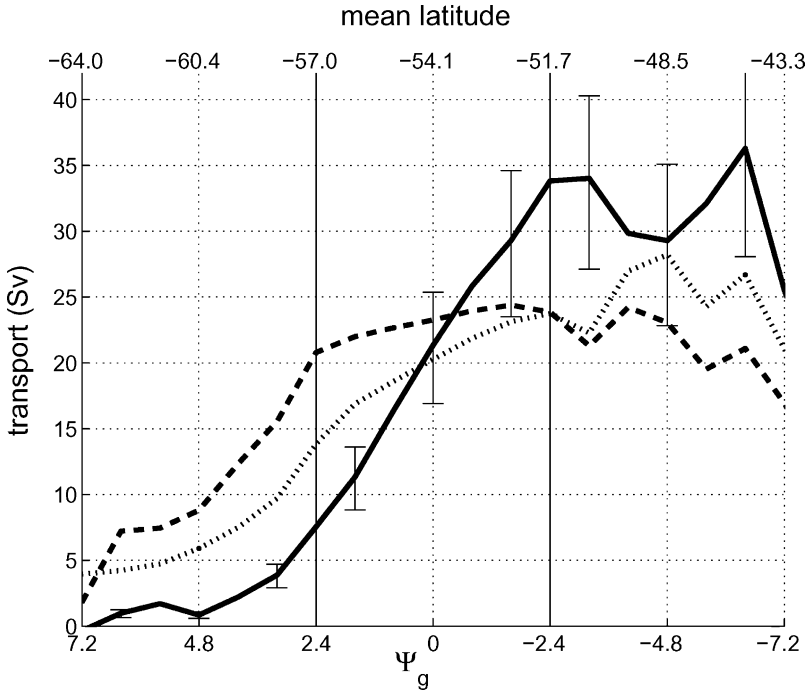$$\Psi_{res}\frac{d\bar{b}_m}{dy} = B, \tag{3}$$

Fig. 6. The Ekman transport $\bar{\Psi} = -\bar{\tau}/\rho_0 f$ and the bolus transport $-\Psi^*$: the dashed line for $\bar{\Psi}$ computed from the SOC winds; the dotted line from HR winds and the solid line is $-\Psi^*$ computed as in KM. The error bars on $-\Psi^*$ are calculated using a 10% error in α and a 1 cm error in the sea-surface height variability, see (5).

where

$$\Psi_{\text{res}} = \bar{\Psi} + \Psi^* = -\frac{\bar{\tau}}{\rho_0 f} + \frac{\overline{v'b'}}{\bar{b}_z}\Bigg|_{z=-h_m}. \tag{4}$$

The first term in (4), $\bar{\Psi}$, is the Eulerian-mean contribution from the Ekman flow, the second, Ψ^*, is the 'bolus transport' at the base of the mixed layer.

Following KM, the terms on the right of (4), $\bar{\Psi}$ and $-\Psi^*$, are plotted in Fig. 6. We plot two etimates of $\bar{\Psi}$ calculated from two different data sets for the winds stress, one from Josey et al. (1998), hereafter SOC winds, and the second from Hellerman and Rosenstein (1983), hereafter HR winds. We use two different wind fields to give some measure of the uncertainty in observed quantities. The eddy flux term is computed as in KM: that is we assume $\overline{v'b'} = -K_m(\mathrm{d}\bar{b}/\mathrm{d}y)$ where K_m is an eddy transfer coefficient at the mixed layer base given by the Keffer and Holloway (1988) formulation

$$K_m = \alpha \frac{g}{|f|}(\overline{(h')^2})^{1/2}, \tag{5}$$

where h' is the sea-surface height variability measured from altimetry and $\alpha = 0.26$ is a constant of proportionality (see Kushner and Held, 1998, for a detailed discussion of the rationale behind (5) and KM for its application to the ACC).

From Fig. 6, we see that the individual terms that make up Ψ_{res} in (4) tend to balance one another to leave a 'residual' that implies northward flow poleward of the ACC (where the wind-stress wins out) and southward flow equatorward of the ACC (where the eddy term wins out)—but note the rather large uncertainty in our estimate of Ψ_{res} due to uncertainties in the wind and our parameterization of $\overline{v'b'}$. In KM, we speculated using (3) that poleward of the ACC there is an implied buoyancy gain by the ocean to balance the equatorward Ekman transport. Similarly, equatorward of the ACC there is an implied buoyancy loss by the ocean to balance the poleward bolus transport. This pattern is in broad agreement with the analysis of COADs data presented in Speer et al. (2000).

3.2. Prediction of thermocline depth

The hypothesis explored by Marshall et al. (2002) and KJM is that the depth of the thermocline in the ACC is controlled by its baroclinic instability: at equilibrium the overturning of isopycnals by $\bar{\Psi}$ was balanced by the counter-overturning tendency, Ψ^*, due to eddies extracting energy from the mean flow.

Let us then attempt to express Ψ^* in terms of h_e. Employing an exponential profile (1) and $\overline{v'b'} = -K_m(\mathrm{d}\bar{b}/\mathrm{d}y)$ we find

$$\Psi^* = -K_m h_e \frac{\mathrm{d}\bar{b}_m/\mathrm{d}y}{\bar{b}_m}, \tag{6}$$

where K_m is the eddy transfer coefficient at the base of the mixed layer. Eq. (6) can be rearranged to solve for h_e giving

$$h_e = -\frac{L}{K_m}\Psi^*, \tag{7}$$

where we have defined the cross-stream length scale of the ACC to be

$$L = \frac{\bar{b}_m}{\mathrm{d}\bar{b}_m/\mathrm{d}y}. \tag{8}$$

From (7) and knowledge of Ψ^*, we can predict h_e given L and the eddy diffusivity K_m.

Further analysis depends critically on how K_m depends on the stratification. Following Green (1970) and Visbeck et al. (1996), we suppose that the eddy diffusivity is given by

$$K_m = \overline{v'l'} = c_e U_0 L_{mix}, \tag{9}$$

where U_0 is the surface thermal wind velocity, L_{mix} a mixing length, and c_e is a constant of proportionality that has been tied down experimentally—see e.g. Jones and Marshall (1997) and Marshall et al. (2002). In (9), we have assumed that the eddy velocity scale $v' \sim U_0$ (appropriate if the eddies garner energy over a deformation scale—see, e.g. the discussion in Section 5 of Held (1999)).

Substituting (9) into (7), we find that

$$h_e = -\left(\frac{1}{c_e}\frac{L}{L_{mix}}\right)\frac{\Psi^*}{U_0}. \tag{10}$$

Thus, the e-folding depth can be related to the surface velocity and Ψ^*. Finally, we express the thermal wind in terms of the buoyancy, that is,

$$U_0 = -\frac{1}{f} \int_{-H}^{-h_\mathrm{m}} \frac{\partial \bar{b}}{\partial y}\, \mathrm{d}z = -\frac{1}{f} \frac{\mathrm{d}}{\mathrm{d}y}(h_\mathrm{e} \bar{b}_\mathrm{m}), \tag{11}$$

where we have assumed that the buoyancy in the abyss is negligible compared to that in the mixed layer. Then (9) yields

$$K_\mathrm{m} = -\frac{c_\mathrm{e} L_\mathrm{mix}}{f} \frac{\mathrm{d}}{\mathrm{d}y}(h_\mathrm{e} \bar{b}_\mathrm{m}). \tag{12}$$

Note that the analysis here differs from KJM because now we allow the e-folding depth to vary across the stream, whereas in KJM it was assumed constant. Substituting (11) into (10) gives

$$h_\mathrm{e} \frac{\mathrm{d}}{\mathrm{d}y}(h_\mathrm{e} \bar{b}_\mathrm{m}) = \left(\frac{1}{c_\mathrm{e}} \frac{L}{L_\mathrm{mix}} \right) f \Psi^*,$$

or

$$\frac{\mathrm{d}}{\mathrm{d}y}(h_\mathrm{e} \bar{b}_\mathrm{m})^2 = \left(\frac{2}{c_\mathrm{e}} \frac{L}{L_\mathrm{mix}} \right) f \Psi^* \bar{b}_\mathrm{m}.$$

Integrating gives

$$(h_\mathrm{e} \bar{b}_\mathrm{m})^2 = \frac{2}{c_\mathrm{e}} \frac{L}{L_\mathrm{mix}} \int_a^y f \Psi^* \bar{b}_\mathrm{m}\, \mathrm{d}y + (h_\mathrm{e} \bar{b}_\mathrm{m})_a^2, \tag{13}$$

where $y = a$ is an arbitrary streamline. In our evaluation of h_e from (13), we choose $y = a$ to be the northern boundary of the ACC and take $(h_\mathrm{e} \bar{b}_\mathrm{m})_a^2$ from the observations. Note that we have assumed that L/L_mix is a constant independent of y.

Rearranging (13) gives our sought-after e-folding scale:

$$h_\mathrm{e} = \frac{\sqrt{\gamma \int_a^y f \Psi^* \bar{b}_\mathrm{m}\, \mathrm{d}y + (h_\mathrm{e} \bar{b}_\mathrm{m})_{y=a}^2}}{\bar{b}_\mathrm{m}}, \tag{14}$$

where

$$\gamma = \frac{2}{c_\mathrm{e}} \frac{L}{L_\mathrm{mix}}. \tag{15}$$

We can now make predictions of thermocline depth, h_e, given an estimate of Ψ^*. In Fig. 7, we plot the diagnosed value of h_e—solid line—using different estimates of Ψ^*.

First, if we accept that we can accurately estimate the diffusivity using (5) then we can use (6) to calculate Ψ^*. The h_e predicted using this value for Ψ^* is given by the dashed line in Fig. 7. The parameter, γ (15) is adjusted to obtain the best fit to the observations of h_e; $\gamma = 180$ was found to yield the best estimate. One interpretation of the excellent prediction shown in Fig. 7 is that the eddy diffusivity given by (9) and (12) is 'compatible' to that obtained following Keffer and Holloway (5).

Another approach would be to construct Ψ^* from observations of surface forcing using (3) and (4). However, we do not have reliable buoyancy flux measurements. Instead we consider
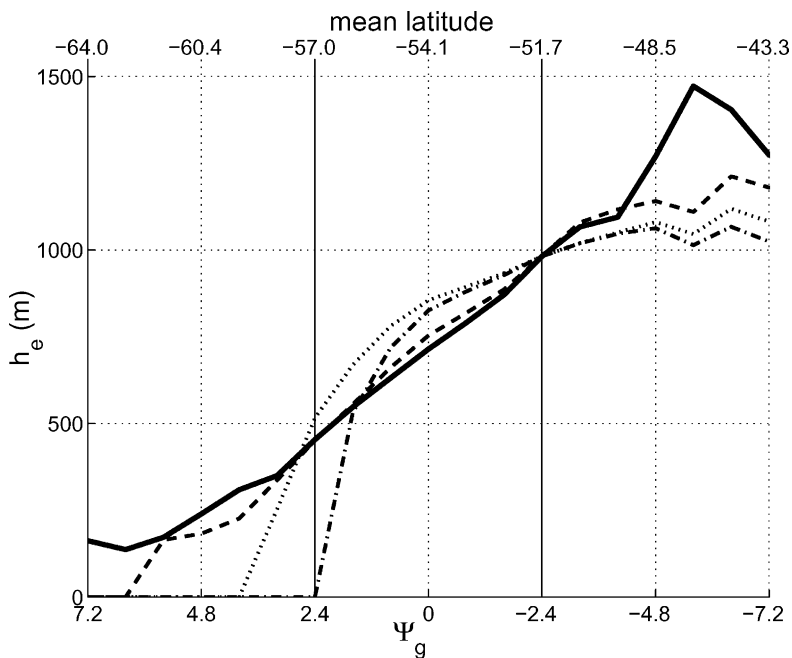
Fig. 7. The mean e-folding depth diagnosed from hydrography (solid line) and calculated from (14) using Ψ^* plotted in Fig. 6 (dashed line) and setting $\Psi^* = -\bar{\Psi} = \bar{\tau}/\rho_0 f$. Dashed–dotted line: SOC winds; dotted line: HR winds.

the limit case in which the surface buoyancy fluxes are assumed to be indistinguishable from zero and so Ψ_{res} vanishes. In this limit,

$$\Psi^* = -\bar{\Psi} = \frac{\bar{\tau}}{\rho_0 f}. \tag{16}$$

when (16) is used for Ψ^* we obtain the predictions of h_e given by the dotted and dashed–doted lines in Fig. 7 for the SOC and HR winds, respectively. The resulting prediction of h_e is consistent with the observations over the northern portion of the ACC but departs markedly from them as we approach the poleward boundary of the ACC. This suggests that here signif-icantly non-zero buoyancy fluxes must support a residual flow—see the previous discussion of Fig. 6.

3.3. Implied baroclinic transport

Given our predictions for thermocline depth, what are the implication for the baroclinic transport of the ACC? The transport of a section of the ACC between $y = a$ and y_1 and below the mixed layer is given by

$$T_{bc} = \int_{-H}^{-h_m} \int_a^{y_1} \bar{u} \, dy \, dz = - \int_{-H}^{-h_m} \int_{-H}^{z} \int_a^{y_1} \frac{1}{f} \frac{\partial \bar{b}}{\partial y} \, dy \, dz' \, dz.$$

We can better understand this formula if we make some reasonable assumptions: we ignore variations in f, we assume the buoyancy (anomaly) vanishes at the bottom, and we can choose 'a' far enough to the south to ensure that $b_{\mathrm{m}}(a)$ essentially vanishes. Under these assumptions we find from (13):

$$T_{bc} = -\frac{1}{f_0}[h_{\mathrm{e}}^2 \bar{b}_{\mathrm{m}}]_a^{y_1} = -\frac{2}{c_{\mathrm{e}}}\frac{L}{L_{\mathrm{m}}}\int_a^{y_1}\Psi^*(y)\frac{\bar{b}_{\mathrm{m}}(y)}{\bar{b}_{\mathrm{m}}(y_1)}\,\mathrm{d}y.$$

We see that the transport depends linearly on Ψ^*. In the limit of vanishing Ψ_{res}, Ψ^* is given by the wind (16) and we recover the result of KJM that the transport of the ACC should depend linearly on the wind stress.

4. Conclusions

We have established that the stratification of the ACC has an exponential form in the region of circumpolar flow. The e-folding depth increases across the ACC from less than 500 m on its poleward flank to more than 1000 m on its equatorial flank. A simple theory that invokes transfer by baroclinic instability to balance patterns of surface buoyancy and wind forcing, can account for the broad features in the stratification documented here in the observations.

Our predictions depend critically on the efficiency of eddies, c_{e}, and the ratio of the eddy mixing scale to the length scale of the front L_{mix}/L which became convolved in to the parameter γ, see (15). To best fit theory and observations of h_{e}, γ was adjusted to 180. The length scale, L, as calculated from (8) is on average 2000 km. There are many different arguments for what sets the mixing length scale, L_{mix}. Some suggest it is proportional to the Rhines scale, which is on average 100 km (see Stammer, 1997), others suggest it is a baroclinic instability scale related to the Rossby deformation scale, estimated from altimetric data to be 50–150 km (see Stammer, 1998). The mixing scale, taken as 2π times either of these estimates, is roughly 500 km, considerably smaller than L. Our calculations then suggest that the eddy efficiency, c_{e}, is $(2/\gamma)(L/L_{\mathrm{mix}}) \approx 0.04$, in agreement with KJM and previous studies (Visbeck et al., 1996; Whitehead et al., 1996; Jones and Marshall, 1997). Eq. (9) then suggests a value K:

$$K_{\mathrm{m}}\,(\mathrm{m}^2\,\mathrm{s}^{-3}) = c_{\mathrm{e}}U_0 L_{\mathrm{mix}} = 0.04 \times 0.08 \times 500 \times 10^3 = 1600,$$

a plausible value of upper ocean eddy diffusivity.

Our predictions are not strongly dependent on small-scale diffusion of buoyancy out of the mixed layer, which has been absorbed into the buoyancy forcing, B. Although not considered here, small-scale diffusivity can influence the strength of the interior stratification and meridional overturning as discussed in KJM and KM, respectively.

What are the implications of our results for the equivalent barotropic form for the mean buoyancy exploited by other authors? First, it is clear that adopting a separable form is not a good approximation because the e-folding depth varies significantly across the ACC. Given the vertical structure of the buoyancy found here, the thermal wind will be equivalent barotropic only if the e-folding depth is constant along streamlines. This is not unreasonable,

as contours of h_e are reasonably coincident with streamlines. If indeed the e-folding depth is constant along streamlines, it can be used as a characteristic variable in, for example, the theory of Killworth and Hughes (2002). Moreover, rather than prescribing that profile, here we have explored its connection with wind, surface buoyancy fluxes and balancing eddy fluxes.

Finally, our discussion in this paper has focused on the observed vertical stratification of the ACC. The residual meridional overturning circulation associated with the ACC is discussed and inferred from observations in another paper (Karsten and Marshall, 2002).

Acknowledgements

References

Danabasoglu, G., McWilliams, J.C., Gent, P., 1994. The role of mesoscale tracer transport in the global ocean circulation. Science 264, 1123–1126.

Döös, K., Webb, D., 1994. The Deacon Cell and other meridional cells of the Southern Ocean. J. Phys. Oceanogr. 24, 429–442.

Gill, 1982. Atmosphere–Ocean Dynamics. Academic Press, New York.

Gille, 1995. Dynamics of the Antarctic Circumpolar Current: evidence for topographic effects from altimeter data and numerical output. Ph.D. Thesis, W.H.O.I., 216 pp.

Gordon, A.L., Molinelli, E., Baker, T., 1978. Large-scale relative dynamic topography of the Southern Ocean. J. Geophys. Res. 83, 3023–3032.

Held, I.M., 1999. The macroturbulence of the troposphere. Tellus 51A–B, 59–70.

Hellerman and Rosenstein, 1983. Normal monthly wind stress over the world ocean with error estimates. J. Phys. Oceanogr. 13, 1093–1104.

Ivchenko, V.O., Richards, K.J., Stevens, D.P., 1996. The dynamics of the Antarctic Circumpolar Current. J. Phys. Oceanogr. 26, 753–774.

Jones, H., Marshall, J., 1997. Restratification after deep convection. J. Phys. Oceanogr. 27, 2276–2287.

Josey, S.A., Kent, E.C., Taylor, P.K., 1998. The Southampton Oceanography Centre (SOC) Ocean–Atmosphere Heat, Momentum and Freshwater Flux Atlas. Southampton Oceanography Centre Rep. 6, Southampton, United Kingdom, 30 pp. + figures.

Karsten, R.H., Marshall, J., 2002. Constructing the residual circulation for the ACC from observations. J. Phys. Oceanogr., to appear.

Karsten, R.H., Jones, H., Marshall, J., 2002. The role of eddy transfer in setting the stratification and transport of a circumpolar current. J. Phys. Oceanogr. 32, 39–54.

Keffer, T., Holloway, G., 1988. Estimating Southern Ocean eddy flux of heat and salt from satellite altimetry. Nature 332, 624–626.

Killworth, P.D., 1992. An equivalent-barotropic mode in the Fine Resolution Antarctic Model. J. Phys. Oceanogr. 22, 1379–1387.

Killworth, P.D., Hughes, C., 2002. The Antarctic Circumpolar Current as a free equivalent-barotropic jet. J. Marine Res., submitted for publication.

Krupitsky, A., Kamenkovich, V.M., Naik, N., Cane, M.A., 1996. A linear equivalent barotropic model of the Antarctic Circumpolar Current with realistic coastlines and bottom topography. J. Phys. Oceanogr. 26, 1803–1824.

Levitus, S., Boyer, T., 1994. World Ocean Atlas 1994 Volume 4: Temperature. NOAA Atlas NESDIS 4. US Department of Commerce, Washington, DC.

Marshall, D., 1997. Subduction of water masses in an eddying ocean. J. Marine Res. 55, 201–222.

Marshall, J., Jones, H., Karsten, R., Wardle, R., 2002. Can eddies set ocean stratification? J. Phys. Oceaongr. 32 26–39.

Marshall, J., Olbers, D., Ross, H., Wolf-Gladrow, D., 1993. Potential vorticity constraints on the dynamics and hydrography of the Southern Ocean. J. Phys. Oceanogr. 23, 465–487.

Olbers, D., Ivchenko, V.O., 2001. On the meridional circulation and balance of momentum in the Southern Ocean of POP. Ocean Dyn. 52, 79–93.

Phillips, H.E., Rintoul, S.R., 2000. Eddy variability and energetics from direct current measurements in the antarctic circumpolar current south of Australia. J. Phys. Oceanogr. 30, 3050–3076.

Rintoul, S.R., Hughes, C., Olbers, D., 2001. The Antarctic Circumpolar Current system. In: Siedler, J.C.G., Gould, J. (Eds.), Ocean Circulation and Climate. Academic Press, New York, pp. 271–302.

Speer, K., Rintoul, S.R., Sloyan, B., 2000. The diabatic Deacon Cell. J. Phys. Oceanogr. 30, 3212–3222.

Stammer, D., 1997. Global characteristics of ocean variability estimated from regional TOPEX/POSEIDON altimeter measurements. J. Phys. Oceanogr. 27, 1743–1769.

Stammer, D., 1998. On eddy characteristics, eddy transports, and mean flow properties. J. Phys. Oceanogr. 28, 727–739.

Visbeck, M., Marshall, J., Jones, H., 1996. Dynamics of isolated convective regions in the ocean. J. Phys. Oceanogr. 26, 1721–1734.

Whitehead, J., Marshall, J., Hufford, G., 1996. Localised convection in rotating stratified fluid. J. Geophys. Res. 101 (C10), 25705–25721.